P5.5 INTRASEASONAL TO DECADAL VARIABILITY OF THE GREATER HORN OF AFRICA

J. Bowden, Fredrick H.M. Semazzi*, R. Anyah, C. Schreck
North Carolina State University, Raleigh, North Carolina

1. INTRODUCTION

The Greater Horn of Africa (GHA) study area is comprised of ten countries: Burundi, Djibouti, Eritrea, Ethiopia, Kenya, Rwanda, Somalia, Sudan, Uganda, and Tanzania. During the OND season, most of the region experiences seasonal rainfall due to the passage of the Inter-Tropical Convergence Zone (ITCZ). The GHA region experiences large interannual rainfall fluctuations which adversely affects the socio-economic and health sectors, including rain-fed agriculture, hydro-electric power, and tourism.

A large percentage of the interannual rainfall variability of GHA is believed to be associated with the global oceans, in particular Pacific driven El Nino Southern Oscillation (ENSO). Many previous studies have examined atmospheric and oceanic anomalies over the Pacific and the corresponding rainfall anomalies over the GHA region. Ogallo (1988) found negative correlation between the OND rainfall and Southern Oscillation Index (SOI) with highest correlations along the Kenyan coast. Farmer (1988) found similar SOI results with highest peak correlation in November. Beltrando and Camberlin (1993) illustrated a positive correlation between rainfall over southern Somalia and Pacific SSTs with negative correlations in September. Similarly, Phillips and McIntrye (2000) have found positive correlation between rainfall over Uganda and Pacific SST during November and December and negative correlations in August and September. The majority of previous studies confirm ENSO's importance in the development of the regional anomalous rainfall, but limited effort has been made to ascertain the relative roles of the potential physical mechanisms responsible for the anomalous rainfall. One of the primary objectives of this study is to investigate possible physical mechanisms with particular interest in the Indian Ocean influence on interannual and intraseasonal rainfall anomalies which has been a major focus of many recent studies.

Saji et al. (1999) found a dipole (zonal) mode of variability within the Indian Ocean, known as the Indian Ocean Dipole/Zonal Mode (IOZM). They found that warm SST anomalies tend to co-exist with easterly wind anomalies over the western tropical Indian Ocean during the positive phase of the IOZM. Webster et al. (1999) have found that the displacement of equatorial convection during the 1997 El Nino event may have been an integral part of the warm SST anomalies in the western Indian Ocean. They suggested that anomalously warm SST over the western Indian Ocean enhance the moist air that penetrates the African continent resulting in increased convection. The convection amplifies the low-level easterly flow further warming the western Indian Ocean via Ekman downwelling. This then strengthens the SST gradient and enhances the rainfall and results in positive feedback. Black et al. (2003) suggested a strong IOZM in which the zonal SST gradient lasts for several months trigger high rainfall over east Africa. Model studies of Goddard and Graham (1999) and Latif et al. (1999) suggested that while the SST variability of the tropical Pacific exerts some influence on the region, it is the atmospheric response to the Indian Ocean variability that play the dominant role in modulating the regional rainfall. Schreck and Semazzi (2004) have examined the existence of El Nino and positive phase of the IOZM during the recent years, 1979-2001. They examine the low-level 850mb wind field by projecting the NCEP wind data onto a given Empirical Orthogonal Function (EOF). The EOF was performed on monthly stratified, seasonally averaged CPC merged Analysis Precipitation (CMAP) data. The weighted wind field illustrated that eastern GHA is dominated by easterly flow from the Indian Ocean during warm ENSO years.

Relatively much less research has been performed to characterize and understand the spatial and temporal intraseasonal variability of ENSO. More over, previous studies on

Corresponding Author Address: Fredrick H.M. Semazzi; Department of Marine, Earth and Atmospheric Sciences, North Carolina State University, Raleigh, NC 27695-8208;
email: fred_semazzi@unity.ncsu.edu

intraseasonal variability tend to focus on wet/dry years associated with ENSO but only limited effort has been made to isolate the affect of ENSO from other modes of variability. Several studies have associated western regions of GHA OND intraseasonal wet conditions with local surface westerly wind anomalies (Anyamba 1984; Davies et al. 1985; Camberlin and Wairoto 1997; Okoola 1999). Mutai and Ward (2000) have suggested that the westerlies may develop 5 days prior to the rainfall event in the equatorial Atlantic and during the event with strengths of about 2-5 m/s. They also have shown that before the rainfall event anomalous near-surface easterlies strengthen over the Indian Ocean, giving the northeast and southeast trades a stronger onshore component. Camberlin and Wairoto (1997) shown that the easterly anomalies are associated with increased rainfall over portions of GHA. The easterly anomalies are a part of the development of the IOZM (Saji et al. 1999). In this investigation we examine the spatial and temporal variability of ENSO and relate the rainfall fluctuations to wind and Sea Surface Temperature Anomalies (SSTA) over the neighboring Indian Ocean.

A recent study of Schreck and Semazzi (2004) has isolated a decadal trend mode during the past two decades using the EOF method. They suggested that the northern sector of GHA is getting wetter while the southern sector is becoming drier. Their analysis explored the possible association of the trend with global warming and found the trend similar to the global warming index constructed by globally averaging surface temperature data from the CRU archive. The trend was also found when performing EOF on the global data set. A similar and consistent trend was found by Dai et al. (1997). They performed EOF on global station rainfall data from 1900-1988 and found a linear increasing trend of about 2.4mm per decade in global average precipitation for the second EOF mode. Our investigation examines a possible explanation that the decadal trend mode is related to the SST over the tropical South Atlantic Ocean. We will also examine the intraseasonal variability of the decadal trend to determine if the trend favors a part of the season.

2. DATA

2.1 CPC Merged Analysis of Precipitation (CMAP)

Rain-gauge measurement is the traditional and oldest method for monitoring rainfall. However, because of practical observational limitations it suffers from numerous gaps in space and time, thus often making its use in climate diagnostic studies less reliable. On the other hand, the estimation of rainfall based on satellites is spatially and temporally comprehensive when calibrated using rain-gauge measurements (Xie and Arkin 1995). Xie and Arkin (1997) have produced a global precipitation data set called CMAP to exploit the combined benefits of gauge observations and satellite proxy data. CMAP is monthly/pentad 2.5° × 2.5° resolution available for January 1979-present.

2.2 Tropical South Atlantic Index (TSAI)

The tropical South Atlantic Index which is also used in our analysis has been constructed from the 1°×1° Optimal Interpolation SST and the Global Sea Ice Sea Surface Temperature data sets. The climatology base for the anomalies is 1951-2000. The SST anomalies are generated from equator - 20°S and 10°E-30°W. The average is then used to compute the index time series (Enfield et al. 1999). The TSAI data can be found at http://www.cdc.noaa.gov/Correlation/tsa.data.

2.3 Reynolds Optimum Interpolation (v2) SST

Our analysis uses the Optimum Interpolation version 2 (OIv2) global SST (Reynolds et al. 2002). The OIv2 SST weekly SST data is a one-degree spatial resolution data set available from November 1981 in which both in-situ and satellite data are available. This newer version of OI SST has reduced errors compared to the older OI SST analysis produced at the National Oceanic and Atmospheric Administration (Reynolds and Smith 1994). The OIv2 SST data is suitable for this study because of its high temporal and spatial resolution.

2.4 NCEP/NCAR wind data

We adopt the National Centers for Environmental Prediction (NCEP) four-dimensional assimilation reanalysis/ National Center for Atmospheric Research (NCAR) wind data to investigate intraseasonal changes in the low-level winds during ENSO/ Indian Ocean Zonal mode. The NCEP/NCAR reanalysis data uses many data sources such as surface, ship, aircraft, and satellite data. The analysis is based on a frozen, state-of-the-art global assimilation system. The data assimilation scheme that was used to generate the data was frozen over the reanalysis

period to avoid the potential climate jumps associated with changes in the real time data assimilation system. However, the reanalysis is still affected by changes in the observing systems (Kalnay et al. 1996). Our study uses the monthly stratified 850hPa/200hPa winds and pentad 925hPa wind data. The latter was provided by the Joint Institute for the study of the Atmosphere and Ocean at the University of the Washington. The pentad mean data are calculated from daily-average data from the NCEP/NCAR Reanalysis Project.

3. Methodology

3.1 Empirical Orthogonal Function (EOF)

This study is primarily based on the analysis of rainfall variability using the EOF method. EOF is a statistical tool that compresses geophysical data fields in space and time. The technique allows us to explain the variance-covariance of the data through a few modes of variability. The modes that account for the largest percent of the original variability are retained after satisfying the traditional statistical significance tests. These modes can be represented by orthogonal spatial patterns (eigenvectors) and corresponding time series (principal components) (Peixoto and Oort 1992).

Our investigation performs EOF on monthly stratified seasonal OND CMAP data for the GHA domain confined within the region bounded by, latitude 13.75°S to 16.25°N and longitude 21.25°E to 53.75°E (Figure 1) and the Indian Ocean of latitude 13.75°S to16.25°N and longitude 39°E to 110°E. The GHA domain chosen is similar to that of Schreck and Semazzi (2004) so that the regional results from the two studies may be compared. We also believe that these results will contribute to the climate prediction activities over the GHA region. We have extended the analysis to the Indian Ocean to gain further understanding of the relationship between the adjacent ocean basin and the GHA rainfall variability. The eigenvectors are supplemented by compositing the seasonal wind fields using the EOF time series amplitudes as the weights. We also perform EOF on pentad CMAP data for the GHA domain to investigate the intraseasonal rainfall variability.

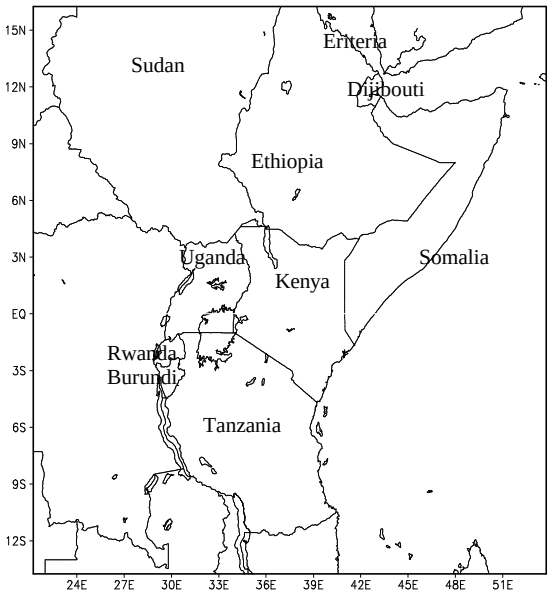

FIG. 1. Orientation map and primary domain for the EOF analysis for the GHA.

4. Results

4.1 Rainfall-Circulation Relationships

Schreck and Semazzi (2004) identified GHA EOF1 as ENSO variability. They describe the low-level 850 hPa circulation [see Figure 14 of Schreck and Semazzi (2004)] as being dominated by inflow from the Indian Ocean and Congo tropical rain forest. They suggested that during warm ENSO events, this may be interpreted as an eastward shift of the upward branch of the Walker circulation that climatologically resides over the Congo tropical rain forest. To further investigate the rainfall-circulation relationships for the low-level circulation, we projected NCEP seasonal mean reanalysis winds at 200hPa onto EOF1 to isolate the three-dimensional circulation associated with warm ENSO events. The upper-level flow (Figure 2) is easterly near equatorial east Africa. It turns westerly over the northern and southern portions of the domain. This is indicative of the barotropic nature of the anomalous circulation with mid-tropospheric latent heat release related to anomalous convection over the GHA. The easterly flow at 200hPa is consistent with the 850hPa easterly flow of Schreck and Semazzi (2004) and perhaps plays a significant role in the occurrence of the wet conditions, particular over the coastal regions, associated with anomalous moisuture flux from the Indian Ocean. Beyond the coastal regions the East African and

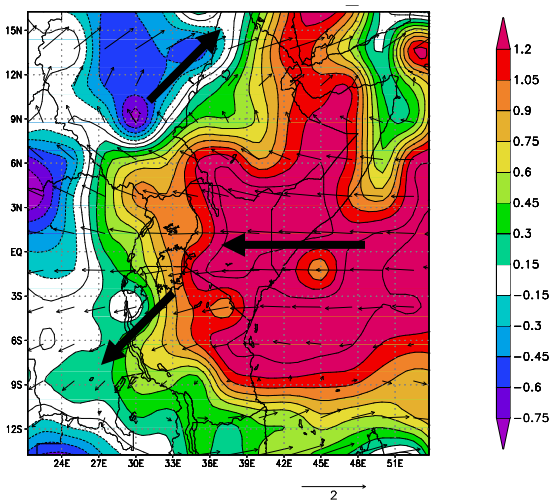

FIG.2. Composite of the 200hPa wind field for EOF1 over the GHA domain. Bold arrows represent the general diffluent easterly flow.

Ethiopian Highlands tend to block the low-level moisture flux. We suggest that the coastal areas benefit from the weakening of the Walker circulation over the Indian Ocean. The weakening of the Walker circulation creates stronger anomalous precipitation over the GHA. As for western GHA, we suggest the Congo tropical rain forest influences the precipitation through the inherently unstable air and the movement of the climatological branch of the Congo Walker Circulation towards western GHA.

The EOF spatial pattern supplemented with wind projections over the Indian Ocean (Figure 3) accounts for 26% of the rainfall variability. The projected low-level winds and eigenmode illustrate similar pattern as the IOZM of Saji et al. (1999). The dominant low-level level flow over the tropical Indian Ocean is easterly. The flow weakens and turns westerly near coastal GHA. Inspection of the Indian Ocean EOF time series and the seasonal OND average of the Dipole Mode Index of Saji et al. 1999 (Figure 4) illustrates that the western Indian Ocean and GHA experience wet conditions during the positive phase of the IOZM. The sensitivity of the domain size and the weights based on the EOF time series provide differing outcomes on the wind field near the GHA coast. The Indian Ocean EOF1 depicts off-shore low-level westerly flow over GHA which is on-shore in the GHA EOF1 analysis. The off-shore flow in the Indian Ocean wind field converges with easterly flow over the western Indian Ocean. The corresponding upper-level circulation is dominated by diffluence which is consistent with low-level convergence over the western Indian Ocean. The upper-level flow over the Indian Ocean is also supportive of a barotropic atmosphere. Overall, the sensitivity of the EOFs illustrates large-scale convergence over the western Indian Ocean confirming the weakening of the Walker Circulation. Locally, the GHA benefits from the weakening of the Walker Circulation possibly explained by enhanced ITCZ convergence through the increase of the climatological northeasterlies. The northeasterlies may also become moisture-laden as they pass over the warm SSTA (Figure 3)..

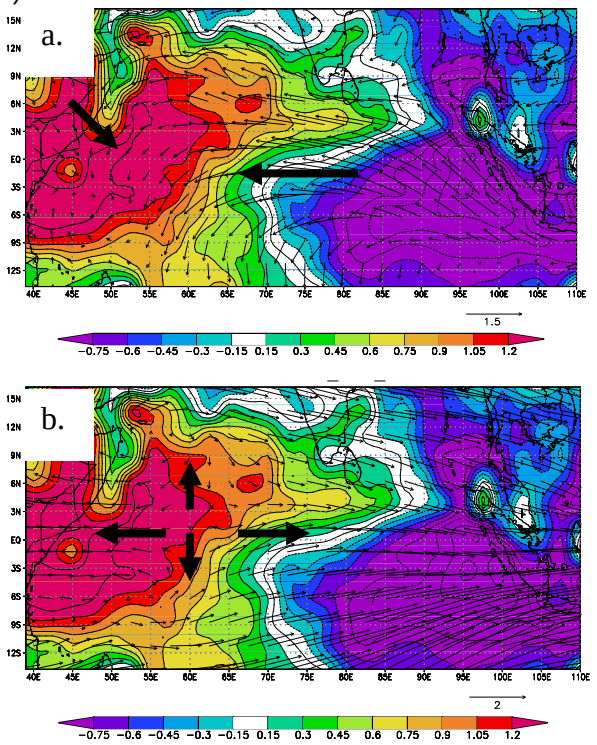

FIG. 3. Weighted wind composite of Indian Ocean EOF1 at a) 850hPa b) 200hPa.

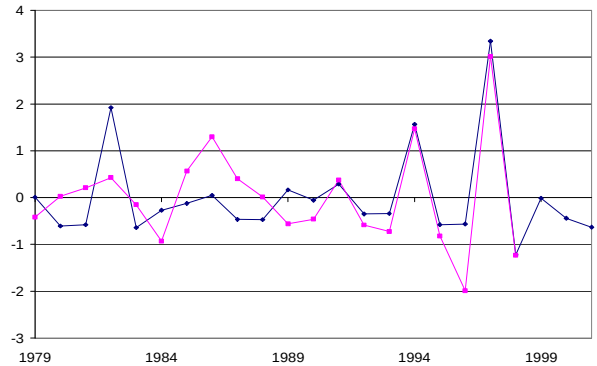

FIG. 4. Comparison of Indian Ocean EOF1 (blue) and Indian Ocean Dipole Mode Index (pink).

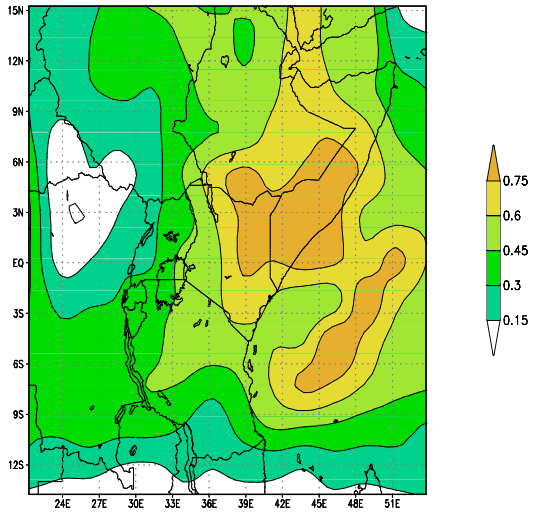

FIG. 5. Pentad EOF1 spatial pattern over GHA.

4.2 Intraseasonal Variability – ENSO

The intraseasonal variability of ENSO was investigated by performing EOF on pentad CMAP data. Pentad EOF1 accounts for 13% of the total variance and has a similar spatial pattern (Figure 5) as seasonal EOF1 [see Figure 5a of Schreck and Semazzi (2004)]. The spatial pattern indicates positive anomalies throughout the entire region of GHA, including Sudan and Ethiopia where the loadings are only slightly positive. Sudan and Ethiopia experienced negative loadings for the seasonal EOF. The loading pattern sign switch over Sudan and Ethiopia possibly can be explained through short-lived events of anomalous rainfall within the season during warm ENSO events. As for the pentad time series, a running mean averaged over a season (18 pentads) is close to the seasonal value (Figure 6). The time series differences are possible because the loading pattern differ slightly from the seasonal analysis.

The pentad time series depicts large peaks within the season. To demonstrate how large the fluctuations are within a season for a given year, we compute a seasonal pentad mean for each year and obtain the departure for each pentad. We then subtract the smallest departure from the largest departure to emphasize the variability of the pentad oscillations over a season (Figure 7). The standard deviation is largest during warm ENSO/positive IOZM events of 1982, 1994 and 1997 with an average standard deviation of five. The exception is in 1991, which is considered to be an ENSO year based on OND seasonal SOI index but experiences near normal fluctuations of about two standard deviations. The La Nina events of 1988, 1998, 1999 and 2000, based on the seasonal SOI index (not shown), have an average standard deviation of 3.4. Therefore, the intraseasonal fluctuations are larger during both the warm and cold phase of ENSO compared to the intraseasonal fluctuations during non-ENSO years.

The El Nino / positive IOZM events of 1982, 1994, and 1997 have the largest intraseasonal fluctuations. Large deviations may be indicative of unusually severe dry and wet spells within the season. We address the question of dry and wet spells during ENSO by compositing the warm ENSO/ positive IOZM events of 1982, 1994, and 1997, (Figure 8) using the pentad EOF time series from two separate EOFs: September 1st – December 15th and October 1st – January 15th. The inclusion of September and January is to allow us to examine the ENSO impact on the onset and withdrawal of the season. The composite calculations also include the estimation

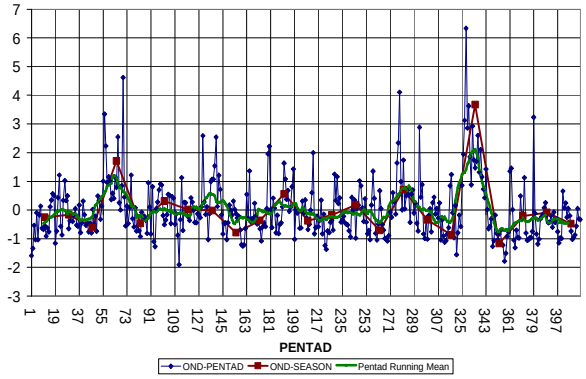

FIG. 6. Intraseasonal time series from 1979-2001 during the OND season (blue), pentad running mean (solid), and seasonal EOF1 (burgundy; adapted from Schreck and Semazzi (2004)). There are 18 pentads per year with the seasonal value centered on pentad 10.

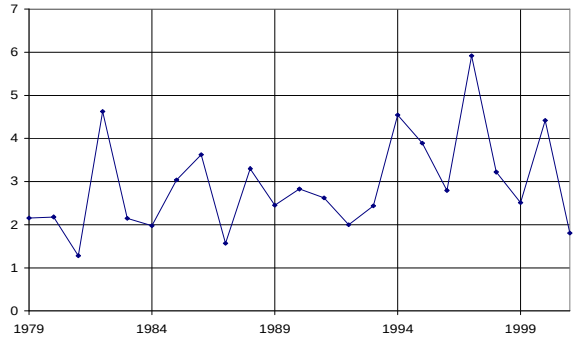

FIG. 7. Anomalies above the pentad mean for each year within the analysis period.

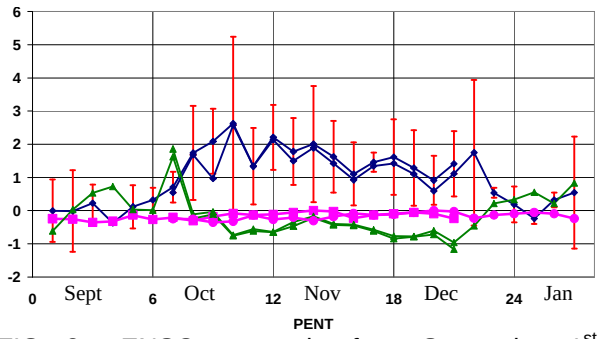

FIG. 8. ENSO composite from September 1st through January 15th. Month begins after every 6th pentad; warm ENSO (blue), cold ENSO (green); normal (pink). Root Mean square error for warm ENSO pentads.

of the root-mean square error associated with each pentad for the warm ENSO events. We include a composite for the cold ENSO events and near normal conditions for comparison. It is important to remember that the composite is representative of only the strongest ENSO/IOZM events during the past two decades, and may not necessarily be representative of the earlier decades.

The general sense of the warm ENSO composite indicate above normal rainfall throughout the entire OND season with a peak in October. The root mean square error of the composite determines the spread in the intensity of the intraseasonal oscillations for each pentad (Figure 8); therefore, the October peak may not be realistic based on the root mean square error. The root mean square error illustrates that the entire season is above normal during the warm phase of ENSO. This result implies that within the GHA region there will be little or no dry spells during the warm phase of ENSO with short-lived extreme rainfall events. The composite of the cold phase of ENSO is one standard deviation below normal throughout most of the season, but the cold phase of ENSO experiences an average deviation of 3.4. The result implies that during the cold phase of ENSO, GHA does experience wet spells although the seasonal average is below normal. The onset and withdrawal of the rainy season during the warm and cold phase of ENSO behave differently. Unfortunately, the error bars are larger than the fluctuations generating low confidence on the differences between warm and cold events.

4.3 Intraseasonal Variability and the Indian Ocean

To build on our previous discussion, we will examine the intraseasonal oscillations of Pentad EOF1 for the 1997 intense El Nino event from September 15th to January 15th. Our focus is on the Indian Ocean intraseasonal variability. We will diagnose the event by stepping through the SST anomalies and the corresponding wind vectors during the season and also attempts to infer its impact on the moisture availability.

The intraseasonal fluctuations over the Indian Ocean for the 1997 El Nino / positive IOZM are shown in Figure 9. The anomalous positive rainfall begins by the first pentad in October. During this time there is a strong positive phase of the IOZM with strong easterly anomalies over the southern equatorial Indian Ocean. Simultaneously there is a patch of warm SST anomalies larger than 2°C near the Somalia coast in association with northeasterly flow. During this time the region is characterized by strong influx of moisture due to strong winds and advection originating from a large area of positive SST anomalies in the western Indian Ocean. Soon after the large influx of moisture there is an increase and peak in the rainfall anomalies centered near the 20th of October. The relationship may suggest a lag of a few weeks between the moisture influx and the peak rainfall anomalies. Soon after the peak rainfall, the wind field weakens decreasing the amount of moisture over the region, even though the SST anomalies near GHA coast increase. By mid-November there are SST anomalies of 1.5°C along coastal GHA with strong northeasterly flow over northern GHA and easterly-southeasterly flow over southern GHA. Again, the intensity of the winds and fetch along with the warm SST anomalies suggest a delayed rainfall peak of approximately two to three weeks. During this period, the rainfall anomalies are on the decline, but a peak in the intraseasonal rainfall is observed two weeks later during the first of December. In mid-to-late December the rainfall anomalies are becoming near normal but anomalous warm SST anomalies are seen along coastal GHA. During this time the flow becomes predominantly northeasterly and parallel to the coast. The northeasterly flow does not favor moisture transport into GHA partially explaining the tendency towards near normal conditions. By mid-January the SST anomalies are very strong along coastal regions of GHA, but the flow is off-shore depriving the region of moisture from the Indian

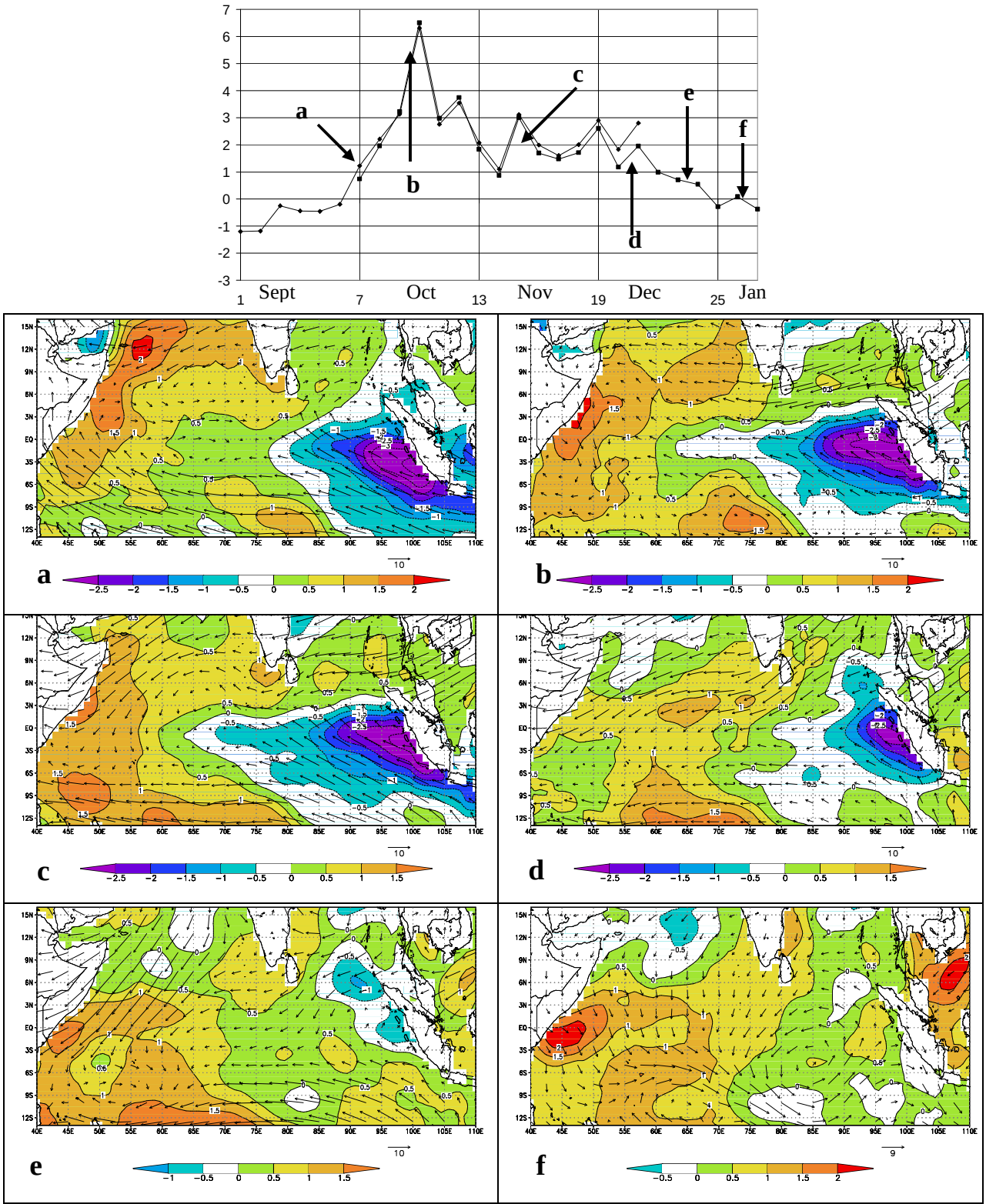

FIG. 9. Overlapping EOF time series from September 1st 1997 – January 15th 1998; Indian Ocean SST anomalies and wind vectors centered closes to the SST anomalies. SST anomalies are for the year 1997 weeks of a) October 5th b) October 19th c) November 16th d) December 14th e) December 28th and f) January 18th 1998.

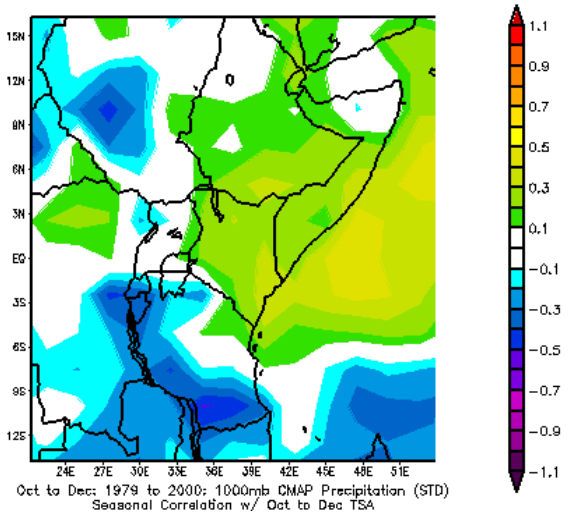

FIG. 10. TSAI and CMAP correlation during the period 1979-2000.

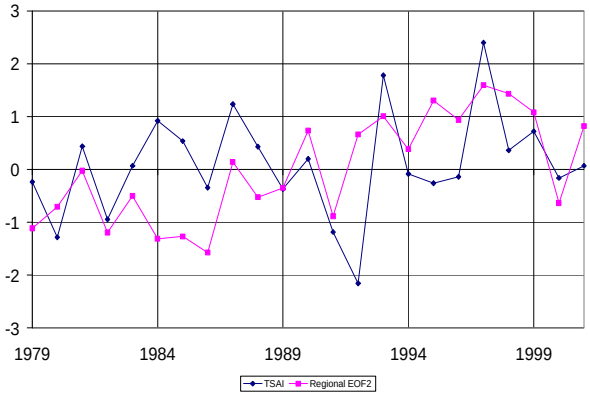

FIG. 11. Comparison between the TSAI (blue) and Seasonal EOF2 (pink).

Ocean consistent with the negative rainfall anomalies. We recognize that there are peaks in rainfall that do not coincide with the Indian Ocean SST and wind field. These rainfall peaks need to be examined in more detail. Overall, the influence of the intraseasonal rainfall peaks with respect to the Indian Ocean during the El Nino and positive IOZM years is believed to be dependent on the following criteria: anomalously warm SST, large fetch, and favorable easterly flow in association with the IOZM.

4.4 Seasonal EOF2 – Decadal Trend

Seasonal EOF2 [see Figure 5b and Figure 12a of Schreck and Semazzi (2004)] is a decadal trend mode with potential connection to global warming. They show the mode to be significant and consistent with global EOF3 and Hadley Climate Research Unit global temperature analysis. We expand on their findings regarding the decadal trend by examining possible connection with the tropical South Atlantic SST which has warmed since the mid-1960's (Levitus et al. 2000). Simple correlation between the TSAI and CMAP (Figure 10) reveal an interesting result. The correlation pattern is similar to that of Schreck and Semazzi (2004) with a dipole loading pattern. Positive correlations give way to positive anomalous rainfall and vice versa. Comparison of the TSAI and Seasonal EOF2 time series (Figure 11) reveals a similar trend. There is the possibility of the trend to be out of phase for some years. For example, in 1984 the tropical South Atlantic was anomalously warm, but the GHA region experienced negative anomalous rainfall.

We suggest that the rainfall variability of the decadal trend is associated with the general warming trend of the tropical South Atlantic. Physically, the moisture capacity of the air near the sea surface increases as the ocean warms. The warmer air is saturated because moisture is readily available from the ocean. It is possible that other ocean basins could be contributing to the trend mode creating problems when considering year to year fluctuation between tropical South Atlantic SST and GHA rainfall anomalies. Future studies will examine the flow associated with the trend and physical explanations for the change in sign between the anomalous rainfall and the SST of the tropical South Atlantic. We expect opposite signs are possible due other ocean basins contribution and the various interactions between the anomalous tropical South Atlantic SST and the corresponding wind field that possibly penetrates the GHA region.

4.5 Intraseasonal Varibility – Decadal Trend

The intraseasonal variability of the decadal trend was analyzed using pentad EOF2. Pentad EOF2 accounts for 8.3% of the total variance and has a similar spatial pattern (Figure 12) as seasonal EOF2. Positive loadings are found over northern GHA and negative loadings over southern sector. The largest positive loadings are located over northern Somalia with the largest negative loadings situated southeast of Lake Victoria. There are a few small differences between pentad EOF2 and seasonal EOF2. The main difference is associated with the transition from positive to negative loadings, with negative loadings extending further north into central Kenya and Sudan for the pentad analysis. As for the time series (Figure 13), a running mean over 18 pentads corresponding to a season resemble the

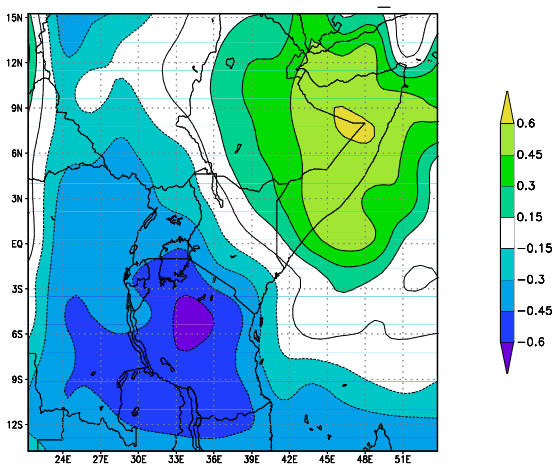

FIG. 12. Pentad EOF2 spatial pattern of GHA.

time series of seasonal EOF2. Again, changes in the pattern are reflected in the time series.

The trend of the intraseasonal variability is diagnosed by rearranging the pentad EOF2 time series. The years are arranged in consecutive order (1979-2001) for each pentad of every month. Each pentad has 23 years with six pentads per month. Overall, the time series represents the trend for each pentad within the season. The intraseasonal monthly time series (Figure 14) depicts October as having the strongest trend mode. Each pentad within October exhibits a decadal trend. The largest trends occur during the last three pentads of October. These pentads have positive and negative anomalies which are as large as two standard deviations. The months of November and December have a weaker trend mode. The weakest trend is during the middle of November with the third pentad having small to no trend. By the end of November into December the trend is more pronounced with positive and negative anomalies reaching two standard deviations. Overall, the strongest intraseasonal variability of the decadal trend is during October. This is the onset month of the rainy season for much of GHA. In conjunction with the spatial pattern, the northern portions of GHA (Somalia, eastern Ethiopia, and northern Kenya) experience an increasing trend in rainfall over the past two decades. We suggest that the increasing trend is possibly related to an early onset of the rainfall over the region. The southern portion of GHA (southern Kenya, Tanzania, Uganda, Congo tropical rain forest, western Sudan) experience decreasing trend in rainfall possibly related to a late start in the seasonal rainfall. The presence of the trend in November and December suggest weaker but similar rainfall pattern to continue throughout the season.

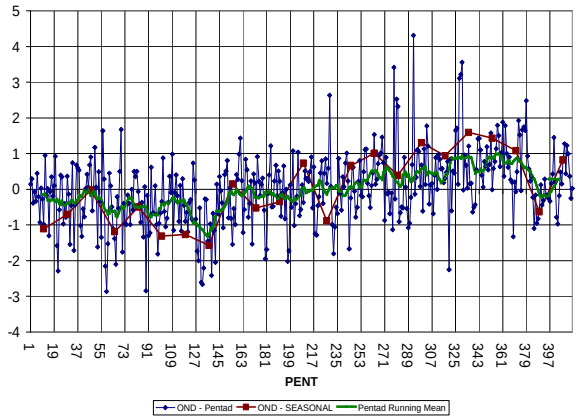

FIG. 13. Comparison between pentad EOF2 (blue), Pentad EOF2 running mean (green), seasonal EOF2 (burgundy; Schreck and Semazzi (2004)). There are 18 pentads per year with the seasonal value centered on the 10th pentad for comparison.

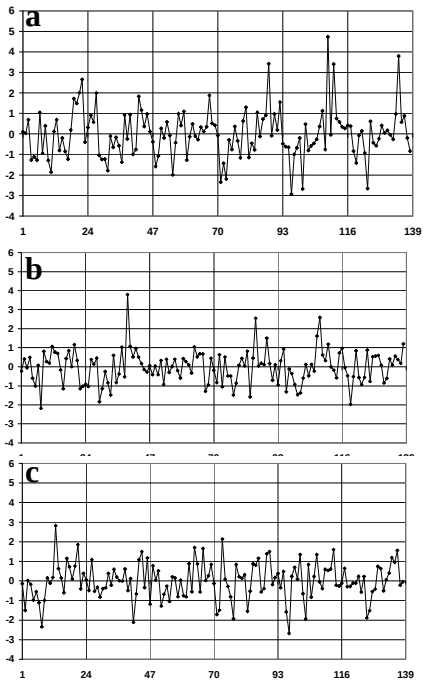

FIG. 14. Intraseasonal variability of the decadal trend for a) October b) November c) December. There are six pentads per month with new pentad beginning at the gridlines.

5. Conclusions

This study investigated the variability of the OND climate of the GHA from intraseasonal to decadal time scales. The variability was diagnosed through EOF analysis on pentad and

monthly stratified CMAP data from 1979-2001. EOF performed on both data sets provided similar spatial and temporal patterns for the first two modes of variability. The dominant mode of variability was identified as ENSO consistent with many previous studies. The second mode of variability represents a decadal trend mode consistent with the global warming index produced by the Hadley Research Center. A diagnosis of the rainfall-circulation relationships has made it possible to better understand the physical processes responsible for anomalous rainfall during ENSO. We also diagnose the intraseasonal variability of ENSO and possible physical forcing responsible for the decadal trend and its intraseasonal variability.

The diagnoses of the rainfall-circulation relationships revealed two braches of the Walker Circulation that contributed to the anomalous rainfall. East of the highland regions, the main contributor to the rainfall anomalies was the weakening of the Indian Ocean Walker Circulation generated by positive SSTA over the western Indian Ocean. We have suggested the rainfall anomalies increased via an anomalously strong northeasterly flow and stronger ITCZ convergence. The stronger low-level northeasterlies also can become moisture-laden through evaporation from the warm ocean surface below. The mountain regions tend to block the moisture-laden low-level northeasterly flow; therefore, we suggested a second branch of the Walker Circulation increases the western GHA rainfall. The climatological branch that resides over the Congo tropical rainfall increases the rainfall western GHA rainfall through the penetration of unstable, moisture laden air of the Congo tropical rainforest. The corresponding upper-level flow illustrated that the entire GHA region convection is sustained through latent heat release generated by anomalous deep convection.

Our study isolated the intraseasonal variability of recent ENSO and co-existing IOZM events. We have found that warm and cold events are not mirror images of one another when considering intraseasonal variability. Composite analysis of recent warm events has illustrated that the entire season tends to be anomalously wet with intense wet spells within the season. On the other hand, cold events represented a drier season with intense dry spells and minor wet spells. The composite analysis demonstrated there is no consistent anomaly during the onset and withdrawal of ENSO events.

We have also investigated the intraseasonal variability of ENSO in relationship to the positive IOZM year of 1997. During the event, the intraseasonal variability of the Indian Ocean was critical to development of several peaks within the season with a lag of approximately two weeks. The peak rainfall events were found to be dependent on warm SST, large fetch, and favorable easterly flow over the western Indian Ocean.

Lastly, we have identified a possible connection of the decadal trend mode to the tropical South Atlantic. Positive loadings were located over northern GHA and negative loadings over southern GHA. We found a similar spatial pattern when correlating CMAP rainfall and the TSAI. We hypothesized that the GHA decadal trend mode benefits from an increase in the SST by increasing the moisture available for penetration into the African continent. We recognized the possibility for year to year fluctuations between the tropical South Atlantic SST and GHA rainfall anomalies to be of opposite sign. We suggested that the year to year fluctuations could be possible because other ocean basins could be contributing to the trend mode, and the various interactions possible between the anomalously warm SST and corresponding wind field. We also have found that the intraseasonal variability of the decadal trend was strongest during the onset month of October. The importance of the strength in October possibly signifies an early onset over northern GHA and a later start in rainfall over southern GHA.

Acknowledgments. We thank Robert Mera for his comments and suggestions. This research was supported by the National Science Foundation (NSF), under grant # ATM-0438116. The computations were performed on the NCAR supercomputing systems. NCAR is supported by the NSF. The post-processing of the results was carried out primarily at the CLIMLAB Laboratory [www.climlab4.meas.ncsu.edu] at North Carolina State University.

References

Anyamba, E.K., 1984: Some aspects of the origin of rainfall deficiency in East Africa. *Proc.of the WMO Regional Scientific Converence on GATE, WAMEX, and Tropical Meteorology*, Dakar, Senegal, pp. 110-112.

Beltrando G. and P. Camberlin, 1993: Interannual variability of rainfall in the eastern Horn of Africa and indicators of atmospheric circulation. *Int. J. Climatol.*, 13, 533-546.

Black, E., J. Slingo, and K.R. Sperber, 2003: An observational study of the relationship between excessively strong short rains in coastal East Africa andIndian Ocean SST. *Mon. Wea. Rev.*, 131, 74-94.

Camberlin, P. and J.G. Wairoto, 1997: Intraseasonal wind anomalies related to wet and dry spells during the long and short rainy seasons in Kenya. *Theor. Appl.Climatol.*, 58, 57-69.

Dai A, I.Y. Fung and A.D.D.Genio (1997): Surface observed global land precipitation variations during 1900-1988. *J. Climate*, 10, 2943-2962.

Davies, T.D., C.E. Vincent, and A.K.C. Beresford, 1985: July-August rainfall in west-central Kenya. *J. Climatol.*, 5, 17-33.

Enfield, D.H. A.M. Mestas, D.A. Myer, L. Cid-Serrano, 1999: How ubiquitous is the dipole relationship in tropical Atlantic sea surface temperature? *J. Geophys. Res.*,104, 7841-7848.

Farmer. G., 1988: Seasonal forecasting of the Kenya Coast short rains. *J. Climatol*., 8, 489-497.

Goddard, L. and N.E. Graham, 1999: Importance of the Indian Ocean for simulating rainfall anomalies over eastern and southern Africa. *J. Geophys .Res*., 104, 19099 19 116.

Kalnay, E. M. Kanamitsu, R. Kistler, W. Collins, D. Deaven, L. Gandin, M. Iredell, S. Saha, G. White, J. Woollen, Y. Zhu, M. Chelliah, W. Ebisuzaki, W. Higgins, J. Janowiak, C.K. Mo, C. Ropelewski, J. Wang, A. Leetmaa, R. Reynolds, R. Jnne., D. Joseph, 1996: The NCEP/NCAR 40-Year Reanalysis Project. *Bull. Amer. Met. Soc*., 77, 437-472.

Levitus, S., J.I. Antonov, T.P. Boyer, and C. Stephens, 2000: Warming of the World Ocean. *Science*, **287**, 2225-2229.

Mutai, C.C. and M.N. Ward, 2000: East African rainfall and the tropical circulation/convection on intraseasonal to interannual timescales. *J. Climate*, **13**, 3915-3939.

Ogallo LJ (1988): Relationships between seasonal rainfall in East Africa and the Southern Oscillation. Int J Climatol 8: 31-43.

Okoola, R.E., 1999: A diagnostic study of the eastern Africa monsoon circulation during the Northern Hemisphere spring season. *Int. J. Climatol*. **19**, 143-168.

Peixoto, J.P., and A.H. Oort, 1992: *Physics of Climate.* American Institute of Physics, NY. pp. 492-496.

Phillips, J. and B. McIntyre, 2000: ENSO and interannual variability in Uganda: Implications for agricultural management. *Int. J. Climatol*., **20**, 171-182.

Reynolds, R.W., T.M. Smith, 1994: Improved global sea surface temperature analyses using optimum interpolation. *J. Climate*, **7**, 929-948.

Reynolds, R.W., W.A. Rayner, T.M. Smith, D.C. Stokes, W. Wang, 2002: An improved in situ and satellite SST analyses for climate. *J.Climate*, **15**, 1609-1625.

Saji, N.H., B.N. Goswami, P.N. Vinayachandran, and T. Yamagata, 1999: A dipole mode in the tropical Indian Ocean. *Nature*. **401**, 360-363.

Schreck, C.J. and F.H.M. Semazzi, 2004: Variability of the recent climate of Eastern Africa. *Int. J. Climtol*., 24, 681-701.

Webster, P.J., A.M. Moore, J.P. Loschnigg, and R.R. Leben, 1999: Coupled ocean-atmosphere dynamics in the Indian Ocean during 1997-98. *Nature*, **401**, 356-360.

Xie, P. and P.A. Arkin, 1995: An intercomparison of gauge observation and satellite estimates of monthly precipitation. *J. App. Met*. **34**, 1143-1160.

Xie, P. and P.A. Arkin, 1997: Global Precipitation: A 17 year monthly analysis based on gauge observations, satellite estimates, and numerical model outputs. *Bull. Amer. Met. Soc*., **78**, 2539-2558.